Supplementary Information

High-purity C_3N quantum dots for enhancing fluorescence detection of metal ions

Huan Yang, [†a,b] Changdao Han, [†c] Jie Jiang, [*a] Pei Li, [*a,b] Liang Chen,[a]

[a]*School of Physical Science and Technology, Ningbo University, Ningbo 315211, China.*

[b]*State Key Laboratory of Surface Physics and Department of Physics, Fudan University, Shanghai 200433, China*

[c]*Department of Optical Engineering, College of Optical, Mechanical and Electrical Engineering, Zhejiang A&F University, Hangzhou 311300, China.*

[†]These authors contributed equally: Huan Yang, and Changdao Han.

*Corresponding author. E-mail: lipei@nbu.edu.cn (P. L.); jiejiang1@nbu.edu.cn (J. J.).

Contents

Eq S1. Yield Calculation

The yield of C_3N QDs can be calculated as the following equation: [S1-S3]

$$\text{yield}=\frac{M_{C_3N\ QDs}}{M_{DAP}} \qquad \textbf{Eq S1}$$

where $M_{C_3N\ QDs}$ is the mass of the obtained C_3N QDs and M_{DAP} is the mass of the DAP powder dissolved in deionized water.

Fig. S1. HRTEM patterns of C_3N QDs

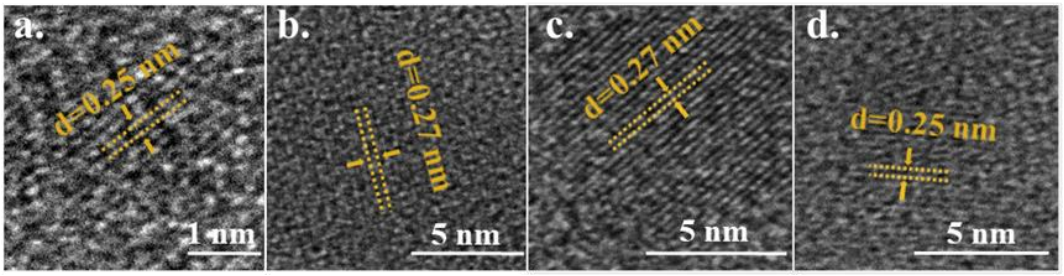

Fig. S1. HRTEM patterns of C_3N QDs.

Fig. S2. Particle Size Distribution of C_3N QDs

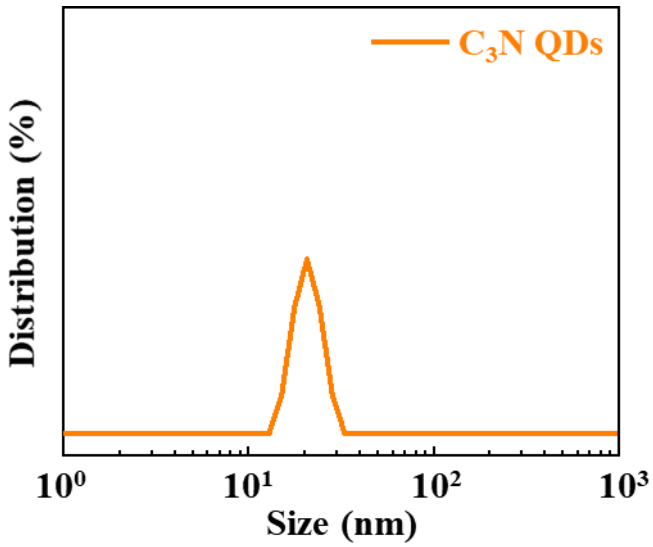

Fig. S2. Particle size distribution of C_3N QDs by nano-particle size analyzer.

Fig. S3. C 1s Spectra of DAP and C_3N QDs

C 1s spectra of DAP and C_3N QDs are shown in Fig. S3. For DAP and C_3N QDs, the high resolution XPS spectra of C 1s can be divided into four components: C-C/C=C with a binding energy at 284.8 eV (grey); C-N at 285.6 eV (blue); C-O at 286.4 eV (purple) and C-NH_2/C=O (green) at 288.7 eV. [S4, S5]

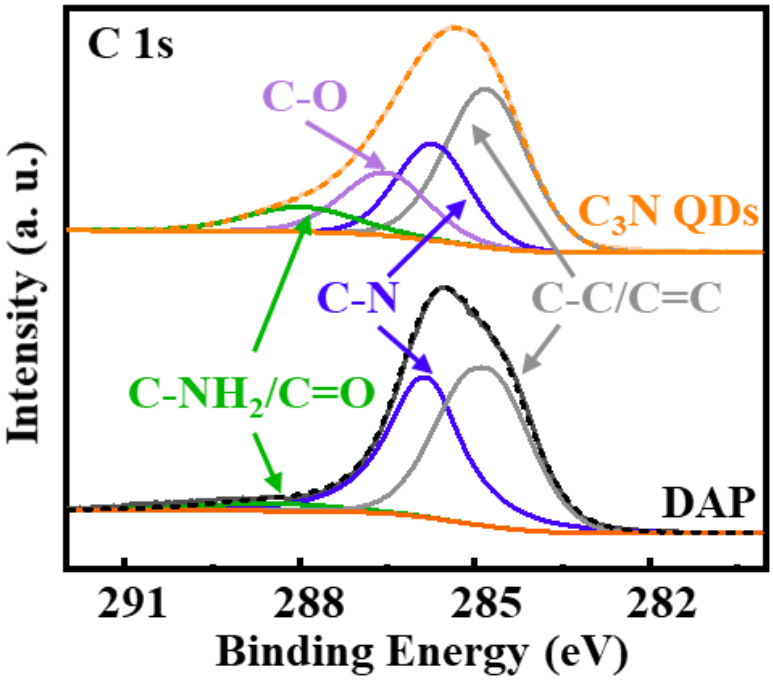

Fig. S3. The C 1s of C_3N QDs and DAP

Table S1. Atomic fractions of C_3N QDs and DAP by XPS

Table S1. Atomic fractions of C_3N QDs and DAP by XPS

Materials	C%	N%	O%
DAP	75.9	21.1	3.0
C_3N QDs	63.4	20.2	16.4

Fig. S4. FTIR Spectra of C_3N QDs and DAP

FTIR spectra of C_3N QDs and DAP are shown in Fig. S4. For C_3N QDs and DAP, the peak at 3437 cm^{-1} may be due to the N-H asymmetric vibration of $-NH_2$. The peaks at 3310, 1497, and 1130 cm^{-1} may be due to the N-H stretching vibration in parahelium structure.[S6] The peak at 3168 cm^{-1} may be due to the C-N stretching vibration of edge benzene ring. The peaks at 1630, 1603, and 1527 cm^{-1} may be due to C=N stretching in phenazine structure.[S7] The peaks at 1640 and 1558 cm^{-1} may be attributed to the C=C stretching in phenazine structure. The peaks at 1334 and 1225 cm^{-1} may be due to the C-N stretching in parahelium structure.

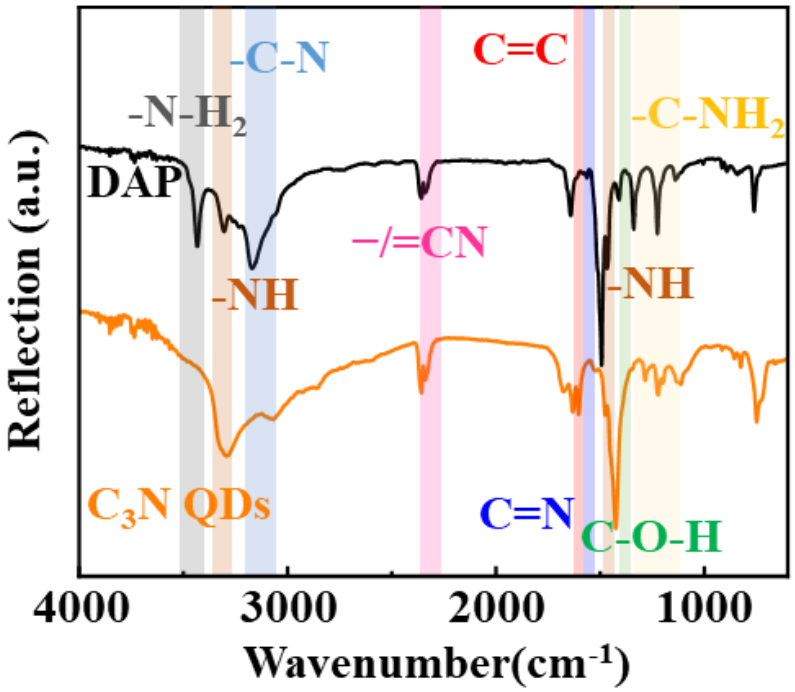

Fig. S4. Fourier transform infrared spectra of C_3N QDs and DAP.

Fig. S5. Lifetime of C_3N QDs

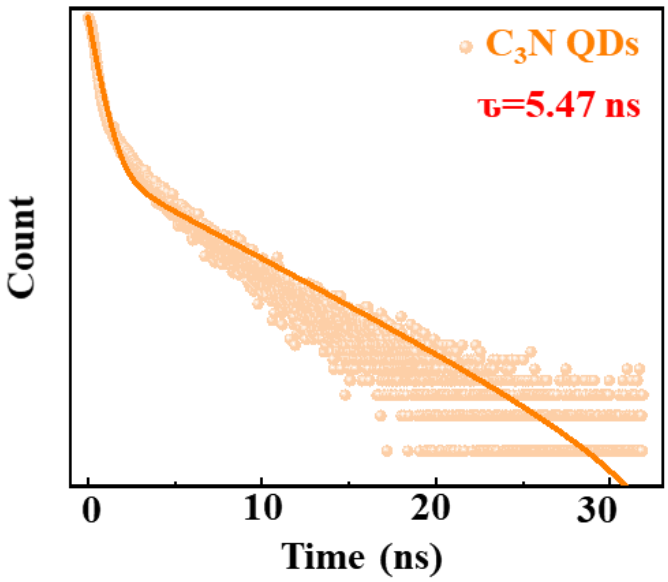

Fig. S5. Time resolved fluorescence spectra of of C_3N QDs.

Considering the background of photons from laser, we adopted bi-exponential decay model to fit the lifetime curves. Based on fitting results, there are two components of the lifetime decay: one is 0.53 ns (94% of the population), the other is 5.47 ns (6% of the population), with χ^2 of 0.98.

Fig. S6. The fluorescence spectra of C_3N QDs w/o Al^{3+}, Ga^{3+}, In^{3+}, and Sc^{3+} ions at different concentrations.

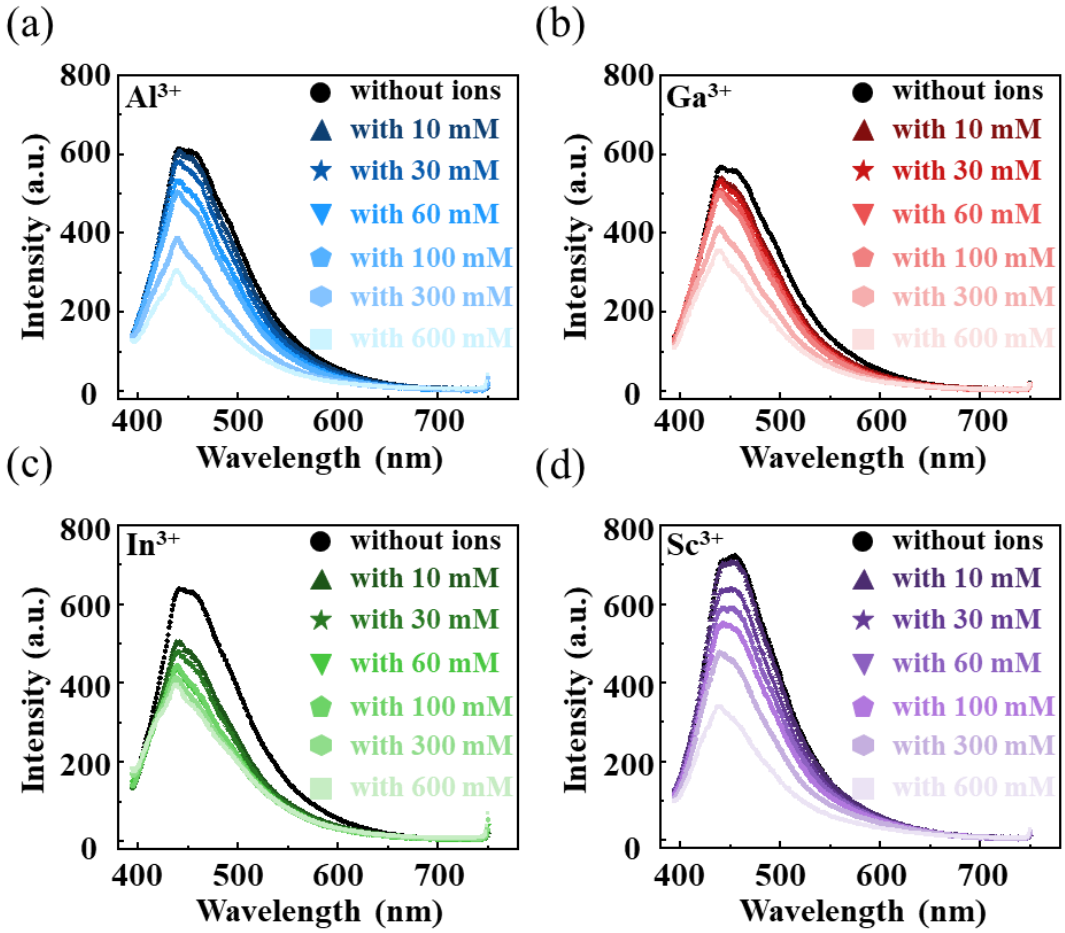

Fig. S6. The fluorescence spectra of C_3N QDs w/o Al^{3+}, Ga^{3+}, In^{3+}, and Sc^{3+} ions at different concentrations. (a) Al^{3+}, (b) Ga^{3+}, (c) In^{3+}, (d) Sc^{3+}.

Table S2. The statistics of fluorescence quenching efficiencies for Al^{3+}/ Ga^{3+}/ In^{3+}/ Sc^{3+}.

Table S2. The statistics of fluorescence quenching efficiencies for Al^{3+}/ Ga^{3+}/ In^{3+}/ Sc^{3+}.

Conditions		**Fluorescence quenching efficiency: $(F-F_0)/F_0$**			
Metal ions	**Ion Concentration (mM)**	**Test 1**	**Test 2**	**Test 3**	**Mean Value**
Al^{3+}	**10**	-0.045	-0.062	-0.060	-0.056 ± 0.009
	30	-0.105	-0.127	-0.121	-0.118 ± 0.011
	60	-0.216	-0.193	-0.206	-0.205 ± 0.011
	100	-0.255	-0.255	-0.273	-0.261 ± 0.010
	300	-0.438	-0.442	-0.465	-0.448 ± 0.015
	600	-0.559	-0.554	-0.578	-0.563 ± 0.013
Ga^{3+}	**10**	-0.250	-0.265	-0.267	-0.261 ± 0.009
	30	-0.319	-0.310	-0.270	-0.300 ± 0.026
	60	-0.334	-0.332	-0.330	-0.332±0.002
	100	-0.379	-0.371	-0.368	-0.373 ± 0.006
	300	-0.396	-0.383	-0.415	-0.398 ± 0.016
	600	-0.362	-0.414	-0.418	-0.398 ± 0.031
In^{3+}	**10**	-0.112	-0.102	-0.122	-0.112 ± 0.010
	30	-0.151	-0.113	-0.154	-0.139 ± 0.023
	60	-0.199	-0.156	-0.178	-0.177 ± 0.021
	100	-0.227	-0.188	-0.215	-0.210 ± 0.020
	300	-0.362	-0.351	-0.360	-0.358 ± 0.006
	600	-0.447	-0.449	-0.461	-0.452 ± 0.007
Sc^{3+}	**10**	-0.011	-0.018	-0.010	-0.013 ± 0.004
	30	-0.075	-0.107	-0.128	-0.103 ± 0.027
	60	-0.145	-0.178	-0.187	-0.170 ± 0.022
	100	-0.200	-0.246	-0.252	-0.233 ± 0.028
	300	-0.340	-0.352	-0.368	-0.353 ± 0.014
	600	-0.547	-0.561	-0.531	-0.547 ± 0.015

* Each test means one of the three independent experiments under same test conditions.

Values following the "±" symbol are the statistical deviation, using as the error bar in **Fig.3.

Table S3. Relative Fluorescence ratios of GQDs or CDs

Table S3. Relative Fluorescence ratios of GQDs or CDs in Fig. 3(b).

Materials	Ion concentrations	$(F-F_0)/F_0$	Ref.
GQD-Al	100 μM	0.60	S8
GQD-Ga	100 mM	0.21	S9
CD-In	10 μM	0.51	S9
GQD-Sc	100 mM	0.31	S9

Fig. S7. The fluorescence spectra of C_3N QDs w/o Li^+, Na^+, K^+, Mg^{2+}, Ca^{2+}, Sr^{2+}, Cu^{2+}, Co^{2+}, Ni^{2+}, Au^{3+}, Fe^{3+}, and Cr^{3+} ions at different concentrations.

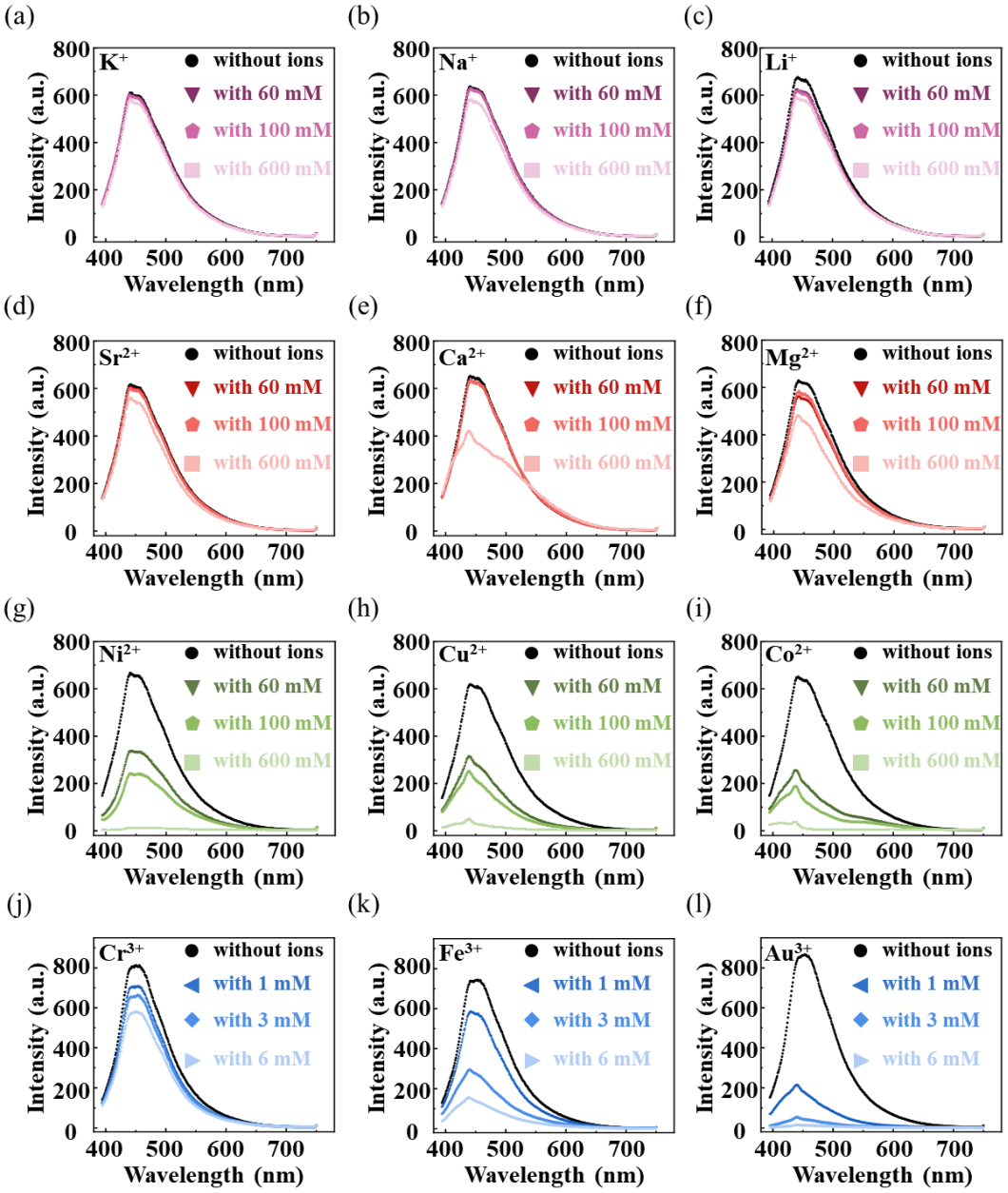

Fig. S7. The fluorescence spectra of C_3N QDs w/o monovalent alkaline metals (Li^+, Na^+, and K^+), divalent alkaline-earth metals (Mg^{2+}, Ca^{2+}, and Sr^{2+}), and multivalent transition metals (Cu^{2+}, Co^{2+}, Ni^{2+}, and Au^{3+}, Fe^{3+}, Cr^{3+}) at different concentrations. (a) K^+, (b) Na^+, (c) Li^+, (d) Sr^{2+}, (e) Ca^{2+}, (f) Mg^{2+}, (g) Ni^{2+}, (h) Cu^{2+}, (i) Co^{2+}, (j) Cr^{3+}, (k) Fe^{3+}, (l) Au^{3+}.

Table S4. The statistics of fluorescence quenching efficiencies for other ions than Al^{3+}/ Ga^{3+}/ In^{3+}/ Sc^{3+}.

Table S4. The statistics of fluorescence quenching efficiencies for other ions than Al^{3+}/ Ga^{3+}/ In^{3+}/ Sc^{3+}.

Conditions		**Fluorescence quenching efficiency: *(F-F₀)/F₀***			
Metal ions	**Ion Concentration (mM)**	**Test 1**	**Test 2**	**Test 3**	**Mean Value**
K^+	**60**	-0.021	-0.014	-0.009	-0.014 ± 0.006
	100	-0.036	-0.021	-0.015	-0.024 ± 0.011
	600	-0.072	-0.066	-0.066	-0.068 ± 0.004
Na^+	**60**	-0.011	-0.006	-0.014	-0.010 ± 0.004
	100	-0.022	-0.017	-0.020	-0.020 ± 0.003
	600	-0.106	-0.096	-0.101	-0.101 ± 0.005
Li^+	**60**	-0.072	-0.060	-0.086	-0.073 ± 0.013
	100	-0.096	-0.082	-0.078	-0.085 ± 0.010
	600	-0.133	-0.122	-0.123	-0.126 ± 0.006
Sr^{2+}	**60**	-0.028	-0.016	-0.022	-0.022 ± 0.006
	100	-0.038	-0.026	-0.036	-0.033 ± 0.006
	600	-0.131	-0.120	-0.129	-0.127 ± 0.006
Ca^{2+}	**60**	-0.021	-0.021	-0.022	-0.022 ± 0.001
	100	-0.018	-0.020	-0.015	-0.018 ± 0.002
	600	-0.206	-0.242	-0.257	-0.235 ± 0.026
Mg^{2+}	**60**	-0.140	-0.115	-0.102	-0.119 ± 0.019
	100	-0.099	-0.091	-0.087	-0.093 ± 0.006
	600	-0.275	-0.280	-0.280	-0.278 ± 0.003
Ni^{2+}	**60**	-0.490	-0.499	-0.499	-0.496 ± 0.005
	100	-0.628	-0.634	-0.634	-0.632 ± 0.003
	600	-0.972	-0.977	-0.977	-0.975 ± 0.003
Cu^{2+}	**60**	-0.555	-0.549	-0.576	-0.560 ± 0.014
	100	-0.665	-0.662	-0.667	-0.664 ± 0.002
	600	-0.948	-0.948	-0.950	-0.949 ± 0.001
Co^{2+}	**60**	-0.650	-0.650	-0.651	-0.650 ± 0.000
	100	-0.757	-0.758	-0.757	-0.758 ± 0.000
	600	-0.958	-0.958	-0.958	-0.958 ± 0.000
Cr^{3+}	**1**	-0.129	-0.186	-0.098	-0.138 ± 0.045
	3	-0.186	-0.191	-0.195	-0.191 ± 0.005
	6	-0.277	-0.288	-0.299	-0.288 ± 0.011

Fe^{3+}	**1**	-0.220	-0.226	-0.278	-0.241 ± 0.032
	3	-0.580	-0.631	-0.643	-0.618 ± 0.033
	6	-0.781	-0.807	-0.809	-0.799 ± 0.015
Au^{3+}	**1**	-0.780	-0.788	-0.792	-0.787 ± 0.006
	3	-0.945	-0.949	-0.952	-0.949 ± 0.004
	6	-0.980	-0.982	-0.983	-0.981 ± 0.001

* Each test means one of the three independent experiments under same test conditions.

Values following the "±" symbol are the statistical deviation, using as the error bar in **Fig.4.

Table S5. The fluorescence changes of carbon-based QDs to various ions.

Table S5. The fluorescence changes of carbon-based QDs to various ions.

Metal ions	Type of carbon-based QDs	Ion concentrations (μM)	Fluorescence change	Ref
Al^{3+}	GQDs	0-12500	**enhance**	S11
	NBD-hnap	0-3		S12
	B-GQDs	0-1.5	**reduce**	S13
	N,B-GQDs	0-400		S14
	Hydroxylated-GQDs	0-10000		S15
In^{3+}	CDs	0-33	**enhance**	S10
	NBD-hnap	0-3		S12
Sc^{3+}	GQDs	0-100	**enhance**	S9
Ga^{3+}	BTC	0-100	**enhance**	S16
	NBD-hnap	0-3		S12
	HT	0-80		S17
	DHTC	0-30		S18
Au^{3+}	CDs	0-15	**reduce**	S19
	C nanodots	0.2-45		S20
Fe^{3+}	N-CDs	0-100	**reduce**	S21
	N-GQDs	0-10000		S22
	Hydroxylated-GQDs	0-50000		S15
Cr^{3+}	Hydroxylated-GQDs	0-40000	**reduce**	S15
Cu^{2+}	CDs@ g-C_3N_4	0-0.01	**enhance**	S23
	N-GQDs	0-200	**reduce**	S22
	Hydroxylated-GQDs	0-25000		S15
	N-CDs	0-100		S24
Co^{2+}	CDs	0-50	**reduce**	S25
	CDs	0-500		S26

References

S1. Y. H. Shin, J. H. Lee, J. H. Yang, J. Park, K. Lee, S. J. Kim, Y. H. Park, and H. Lee, Small, 2014, 10.5, 866-870.

S2. Y. Q. Sun, S. Q. Wang, C. Li, P. H. Luo, L. Tao, Y. Wei, and G. Q. Shi, Physical Chemistry Chemical Physics, 2013, 15.24, 9907-9913.

S3. H. G. Huang, S. W. Yang, Q. T. Li, Y. C. Yang, G. Wang, X. F. You, B. H. Mao, H. S. Wang, Y. Ma, P. He, Z. Liu, G. Q. Ding, and X. M. Xie, Langmuir, 2018, 34.1, 250-258.

S4. S. Liu, J. Q. Tian, L. Wang, Y. W. Zhang, X. Y. Qin, Y. L. Luo, A. M. Asiri, A. O. Al-Youbi, X. P. Sun, Advanced materials, 2012, 24.15, 2037-2 041.

S5. L. Cao, M. H. Zan, F. M. Chen, X. Y. Kou, Y. L. Liu, P. Y. Wang, Q. M ei, Z. Hou, W. F. Dong, L. Li, Carbon, 2022, 194, 42-51.

S6. S. W. Yang, W. Li, C. C Ye, G. Wang, H. Tian, C. Zhu, P. He, G. Q. Di ng, X. M. Xie, Y. Liu, Advanced Materials, 2017, 29.16, 1605625.

S7. Z. H. Tian, T. Heil, J. Schmidt, S. K. Cao, and M. Antonietti, ACS applie d materials & interfaces, 2020, 12.11, 13127-13133.

S8. B. B. Chen, R. S. Li, M. L. Liu, H. Y. Zou, H. Liu, C. Z. Huang, Talant a., 2018, 178, 172-177.

S9. J. Yang, P. Li, Z. L. Song, J. Li, H. Yang, Y. Fan, L. Li, C. Xu, J. L. C hen, L. Chen, Appl. Surf. Sci., 2022, 593, 153367.

S10. S. Pawar, S. Kaja and A. Nag, ACS omega., 2020, 5.14, 8362-8372.

S11. M. M. Yao K. Huang, Z. H. Deng, Y. Wen, Y. L. Yuan, F. Nie, H. Wan g, F. Y. Du, and Y. Zhang, Analyst, 2020, 145, 6981-6986.

S12. Q. X. Zheng, F. Ding, X. J. Hu, J. Y. Feng, J. L. Shen, X. J. He, Bioor ganic Chemistry, 2021, 109, 0045-2068.

S13. W. Li, L. Zhang, N. Jiang, Y. Q. Chen, J. Gao, J. H. Zhang, B. S. Yang, andJ. L. Liu, Molecules, 2022, 27, 6771.

S14. X. Li, L. X. Zhao, Y. H. Wu, A. Zhou, X. F. Jiang, Y. Zhan, Z. G. Sun, Spectrochimica Acta Part A: Molecular and Biomolecular Spectroscopy, 20 22, 282, 1386-1425,

S15. Q. Ge, W. H. Kong, X. Q. Liu, Y. M. Wang, L. F. Wang, N. Ma, Y. Li, International Journal of Minerals Metallurgy and Materials, 2020, 27, 91–9 9.

S16. H. Y. Xiang, T. R. Wang, S. X. Tang, Y. J. Wang, N. Xiao, Spectrochimi ca Acta Part A: Molecular and Biomolecular Spectroscopy, 2022, 267, 138 6-1425.

S17. L. J. Yang, M. X. Li, Y. Y. Wang, Y. Zhang, Z. P. Liu, S. T. Ruan, Z. L. Wang, and S. F. Wang, Analyst, 2021, 146, 7294-7305.

S18. J. S. Heo, D. Gil, C. Kim, Luminescence, 2022, 37, 684-690.

S19. Y. Guo, T. Li, L. W. Xie, X. Tong, C. Tang, S. Y. Shi, Analytical And Bioanalytical Chemistry, 2021, 413, 935–943.

S20. Y. Z. Fan, S. G. Liu, Y. Zhang, W. Ren, Z. Sun, B. L. Li, H. Q. Luo,

N. B. Li, Applied Surface Science, 2020, 526, 0169-4332.
S21. M. H. Qin, S. Y. Zong, P. Zhang, J. Y. Li, Journal of Materials Science, 2023, 58, 7559–7570
S22. Q. Yao, H. Y. Wu, Y. H. Jin, C. L. Wang, R. T. Zhang, Y. J. Lin, S. J. Wu, Y. H. Hu, Current Applied Physics, 2022, 41, 1567-1739.
S23. K. Radhakrishnan, S. Sivanesan, P. Panneerselvam, Journal of Photochemis try and Photobiology A: Chemistry, 2020, 389, 1010-6030.
S24. B. Gao, D. Chen, B. L. Gu, T. Wang, Z. H. Wang, F. Xie, Y. S. Yang, Q. L. Guo, G. Wang, Current Applied Physics, 2020, 20, 1567-1739.
S25. C. Y. Li, N. Li, L. Yang, L. Liu, D. H. Zhang, Spectrochimica Acta Part A: Molecular and Biomolecular Spectroscopy, 2024, 309, 1386-1425.
S26. G. K. Hu, L. Ge, Y. Y. Li, M. Mukhtar, B. Shen, D. S. Yang, J. G. Li, Journal of Colloid and Interface Science, 2020, 579, 0021-9797.